Optical-Field-Driven Electron Tunneling in Metal-Insulator-Metal Nano-junction

--Manuscript Draft--

Manuscript Number:	advs.202101572
Article Type:	Research Article
Corresponding Author:	Qing Dai, Ph.D. National Center for Nanoscience and Technology, China Beijing, Beijing CHINA
Corresponding Author E-Mail:	daiq@nanoctr.cn
Order of Authors:	Qing Dai, Ph.D.
	Shenghan Zhou
	Xiangdong Guo
	Ke Chen
	Matthew Thomas Cole
	Zhenjun Li
	Chi Li
Keywords:	MIM nano-junction; optical-field-driven tunneling; high nonlinearity; ultrafast electronics
Manuscript Classifications:	Physical Sciences & Engineering; PHOTONICS (incl. non-visible wavelengths) - optical properties, optoelectronic devices (LEDs, photodetectors), optical sensors/detectors, plasmonics, metamaterials
Section/Category:	
Abstract:	Optical-field driven electron tunneling in nano-junctions has made demonstrable progress towards the development of ultrafast charge transport devices at sub-femtosecond time scales, and in doing so have evidenced great potential as a springboard technology for the next generation of on-chip “lightwave electronics”. Here, we report our empirical findings on photocurrent the high nonlinearity in metal-insulator-metal (MIM) nano-junctions driven by ultrafast optical pulses in the strong optical-field regime. In the present MIM device we have identified a 14 th power-law scaling, never achieved before in any known solid-state device. This work lays important technological foundations for the development of a new generation of ultracompact and ultrafast electronics devices that operate with sub-optical-cycle response times.
Suggested Reviewers:	
Opposed Reviewers:	
Author Comments:	
Additional Information:	
Question	**Response**
Please submit a plain text version of your cover letter here.	Dear Editor, Thank you very much for your kind invitation. Please find attached our manuscript entitled “Optical-Field-Driven Electron Tunneling in Metal-Insulator-Metal Nano-junction” for your consideration for publication in Advanced Science. Optical-field driven electron tunneling in nano-junctions has made demonstrable progress towards the development of ultrafast charge transport devices at sub-femtosecond time scales. However, previously reported ultrafast electron tunneling devices have suffered from relatively high vacuum barrier (commonly ~5 eV), and

	when coupled to the need for access to the optical-field driven regime only occurs at high field-strength (>10 V/nm), has resulted in photocurrent nonlinearities reducing to very low values, typically ~2. Here, we report our empirical findings on photocurrent the high nonlinearity in metal-insulator-metal (MIM) nano-junctions driven by ultrafast optical pulses in the strong optical-field regime. With the assistance of a DC bias voltage, the optical-field-driven tunneling regime has been achieved with transport showing a high nonlinearity of up to 14 in the current-power (I-P) curve (P7), never achieved before in any known solid-state device. This highly nonlinearity constitutes an important leap in our understanding of transport in MIMs devices and contributes towards the realization of ultracompact and ultrafast PHz solid states electronics devices, such as CEP detectors. We are confident that this paper will trigger the research upsurge of lightwave electronics based on optical-field-driven electron tunneling devices. This work lays important technological foundations for the development of a new generation of ultracompact and ultrafast electronics devices that operate with sub-optical-cycle response times. We very much look forward to hearing from you. Yours sincerely, Qing Dai, Professor at National Center of Nano Science and Technology Beijing, China
Does the research described in this manuscript include animal experiments?	No
Does the research described in this manuscript include human research participants (including for experiments with sensors or wearable technologies) or tissue samples from human subjects (including blood or sweat)?	No
Do you or any of your co-authors have a conflict of interest to declare?	No. The authors declare no conflict of interest.
This journal's Expects Data Policy requires a Data Availability Statement (even if no data are shared), which will be published alongside your manuscript if it is accepted for publication. Do you choose to share the research data described in this manuscript?	No. Research data are not shared.

Dear Editor,

Thank you very much for your kind invitation. Please find attached our manuscript entitled "*Optical-Field-Driven Electron Tunneling in Metal-Insulator-Metal Nano-junction*" for your consideration for publication in *Advanced Science*.

Optical-field driven electron tunneling in nano-junctions has made demonstrable progress towards the development of ultrafast charge transport devices at sub-femtosecond time scales. However, previously reported ultrafast electron tunneling devices have suffered from relatively high vacuum barrier (commonly ~5 eV), and when coupled to the need for access to the optical-field driven regime only occurs at high field-strength (>10 V/nm), has resulted in photocurrent nonlinearities reducing to very low values, typically ~2.

Here, we report our empirical findings on photocurrent the high nonlinearity in metal-insulator-metal (MIM) nano-junctions driven by ultrafast optical pulses in the strong optical-field regime. With the assistance of a DC bias voltage, the optical-field-driven tunneling regime has been achieved with transport showing a high nonlinearity of up to 14 in the current-power (I-P) curve (P^7), never achieved before in any known solid-state device. This highly nonlinearity constitutes an important leap in our understanding of transport in MIMs devices and contributes towards the realization of ultracompact and ultrafast PHz solid states electronics devices, such as CEP detectors.

We are confident that this paper will trigger the research upsurge of lightwave electronics based on optical-field-driven electron tunneling devices. This work lays important technological foundations for the development of a new generation of ultracompact and ultrafast electronics devices that operate with sub-optical-cycle response times.

We very much look forward to hearing from you.

Yours sincerely,

Qing Dai,
Professor at National Center of Nano Science and Technology
Beijing, China

DOI: 10.1002/ ((please add manuscript number))
Research Article

Optical-Field-Driven Electron Tunneling in Metal-Insulator-Metal Nano-junction

Shenghan Zhou, Xiangdong Guo, Ke Chen, Matthew Thomas Cole, Zhenjun Li, Chi Li, and Qing Dai**

S. H. Zhou, Dr. X. D. Guo, K. Chen, Dr. Z. J. Li, Prof. C. Li, Prof. Q. Dai
CAS Key Laboratory of Nanophotonic Materials and Devices, CAS Center for Excellence in Nanoscience, National Center for Nanoscience and Technology, Beijing 100190, P. R. China
E-mail: daiq@nanoctr.cn; lichi@nanoctr.cn
S. H. Zhou, X. D. Guo, K. Chen, Dr. Z. J. Li, Prof. C. Li, Prof. Q. Dai
University of Chinese Academy of Sciences, Beijing 100049, P. R. China
Dr. M. T. Cole
Department of Electronic and Electrical Engineering, University of Bath, BA2 7AY, UK

Keywords: MIM nano-junction; optical-field-driven tunneling; high nonlinearity; ultrafast electronics

Abstract

Optical-field driven electron tunneling in nano-junctions has made demonstrable progress towards the development of ultrafast charge transport devices at sub-femtosecond time scales, and in doing so have evidenced great potential as a springboard technology for the next generation of on-chip "lightwave electronics".[1] Here, we report our empirical findings on photocurrent the high nonlinearity in metal-insulator-metal (MIM) nano-junctions driven by ultrafast optical pulses in the strong optical-field regime. In the present MIM device we have identified a 14^{th} power-law scaling, never achieved before in any known solid-state device. This work lays important technological foundations for the development of a new generation

of ultracompact and ultrafast electronics devices that operate with sub-optical-cycle response times.[2-10]

The use of strong optical-field in ultrashort pulsed lasers are today commonly employed in steering electrons at sub-femtosecond time scales.[11-15] More recently, interest has focused on utilizing such ultrafast electrons as carriers in solid-state electronic devices due to their potential to overcome operation speed limitations plaguing present-day electronics. Such approaches are widely heralded as a viable means of realizing a new generation of petahertz electronics.[13, 14, 16] For this purpose, several fundamental types of optical-field driven ultrafast electron devices have been proposed and demonstrated,[17-19] among which nano-junction tunneling devices are perhaps some of the most promising given the case with which the strong optical-field enhancement can be achieved in the nano-junction.

A key requirement for ultrafast devices is the need for highly nonlinearity, with a highly sensitive photocurrent modulation capable of sub-femtosecond on-off transients. Previously reported ultrafast electron tunneling devices have suffered from relatively high vacuum barrier (commonly ~5 eV),[17-21] and when coupled to the need for access to the optical-field driven regime only occurs at high field-strength (>10 V/nm), has resulted in photocurrent nonlinearities reducing to very low values, typically ~2.[17, 20, 21] Although devices with this performance level have demonstrable potential in future petahertz electronics; specifically carrier-envelope phase (CEP) detector,[14, 22] this nonlinearity must be further increased in order to greatly enhance detection sensitivity.

Here, we report on the measured ultrafast laser driven photocurrent in a nanoscale MIM

device. One of the advantages of the present MIM structure is that the tunneling barrier can be band-optimized by selecting sandwiches created from a plethora of insulating and conducting materials.[23] Compared to previously reported nano-junction devices, the tunneling barrier of the present device is, as a result, greatly lowered to 1.73 eV, thereby enabling improved access to the optical-driven tunneling regime at a much lower field-strengthen of ~5 V/nm.[17] With the assistance of a DC bias voltage, the optical-field-driven tunneling regime has here been achieved with transport showing a high nonlinearity of up to 14 in the current-power (I-P) curve (P^7), a finding we further corroborate via polarization-dependent experiments. This highly nonlinearity constitutes an important leap in our understanding of transport in MIMs devices and contributes towards the realization of ultracompact and ultrafast PHz solid states electronics devices, such as CEP detectors.

Similar to structures formed elsewhere,[17, 23] the present MIM structure, as shown in **Figure 1a**, consists of a top electrode formed from a 3/60 nm Ti /Au layer, followed by an insulator formed from an 8 nm-thick ALD-grown nano-Al_2O_3 film, and finally a 60 nm-thick Au layer which forms the bottom electrode. Using electron beam lithography, the top electrode is subsequently shaped into nanotriangle structures of 300×400 nm, which serve to focus the free-space optical-field to a nanoscale hotspot at the nanotriangle tip. Figure 1a depicts the photoemission process of a single unit of the asymmetric MIM structure excited by a femtosecond laser pulse. A typical fabricated device is shown in **Figure 1b**. The focused optical-field is then coupled to the MIM structure to achieve a high field enhancement factor within the nanogap. A linear polarized, ultrafast laser with an FWHM pulse width of 140 fs, 80 MHz repetition rate, a tunable wavelength (680-1050 nm), and a spot size of ~2.5 μm

(FWHM), was illuminated vertically onto the sample surface. Photo-excited electrons were then attracted by the combined effects of a DC electric-field and the incident optical-field, with liberated electrons emitted from one electrode to the counter electrode. Although the photocurrent is nominally bidirectional, in the present work we focus on exploring those photocurrents from the top nano-triangular structures to the bottom flat electrode in order to investigate the field enhancement impacts of the top nanotriangle electrode (Figure S1a). To obtain a measurable photocurrent, the top electrode consists of a series of parallel Au stripes (the laser irradiation area ~3 μm) with asymmetric nanotriangle structures and the total measured current is the sum of all photo-excited nanotriangle photocurrent contributions.

As shown in **Figure 1c**, we measure both the tunnel current I_{dc} without laser illumination and the photoemission current $I_{emission}$ during laser excitation as a function of different optical power (P). The DC current without laser illumination shows no measurable signal (I <0.1 pA, commensurate with the noise floor of the precision ammeter used). However, a remarkable current-voltage (I-V) characteristic evolves with increasing laser illumination. The device rectifies, an effect which we attribute to the asymmetric in the junction's material composition (Ti/Au-Al_2O_3-Au). The zero current point is at around 0.8V, suggesting a Schottky barrier height difference of 0.8 eV. This is consistent with values reported elsewhere as well as our measured work function difference between the Au (5.1 eV) and Ti (4.33 eV) in the present structure.[24, 25] The wavelength-dependent photocurrent spectrum (**Figure 1d**) suggests a plasmon resonant peak of 880 nm for the given device geometry, as shown in the inset of Figure 1d. **Figure 1e** shows the simulated electromagnetic field distribution in the Ti/Au-Al_2O_3 interface of the MIM device at λ=880 nm. The field enhancement at 880 nm

(β=41.7) is notably enhanced compared to that at 730 nm (Figure S1b, β=27.6), corresponding to the photocurrent spectrum shown in Figure 1d.

The MIMs operation principle is illustrated in **Figure 2**. The equilibrium state (no bias, no illumination) is shown in **Figure 2a**. The barrier height is approximately equal to the difference in the work function for Ti (W_{Ti} = 4.33 eV) and the electron affinity of the crystalline Al_2O_3 (χ_{Al2O3} = 2.6 eV), that is, φ_B = 1.73 eV. When biased, but without laser illumination, the device operates in the conventional static-field-driven electron tunneling regime.[26, 27] Dependent on the bias voltage, this static-field-driven electron tunneling may transit from direct tunneling (rectangular barrier) to F-N tunneling (triangular barrier, **Figure 2b**). Under ultrafast laser illumination at relative weak power (<0.3 mW), photon-assisted tunneling dominates[28]—electrons around the Fermi level absorb one or more photons exciting them into a higher energy level and then tunnel into the conduction band of Al_2O_3, assisted by the static-field. When driven at medium optical powers (<0.6 mW), the device operation adopts multiphoton photoemission[21, 29-31]—electron around the Fermi level (E_f) absorb additional photons and in doing so obtain sufficient energy to overcome the surface barrier entirely (**Figure 2c**). In the present device structure, as the Schottky barrier height is ~1.73 eV, one-photon-assisted tunneling and two-photon photoemission likely dominate under the optical pulsed excitation. When illuminated with a much more intense laser (>0.6 mW), the strength of the optical-field in the nano-junction is likely sufficiently high (~5 V/nm) to perturb the Schottky barrier such that the electrons around E_f may tunnel through the periodically narrowed barrier as a result of the oscillating optical-field (**Figure 2d**).[13, 14, 32, 33]

An example of a typical I-V curve measured for devices illuminated with different laser powers is shown in **Figure 3**. **Figure 3a** shows the tunneling behavior without laser excitation. Below 1V, the I-V curve shows widely reported linear behavior associated with conventional direct tunneling.[34, 35] Conversely, at the higher bias (>1V), the tunneling behaves increasingly nonlinear, adopting more F-N-like tunneling as one would expect for an electron dense emitting surface. This is further evidenced by the F-N fitting of the I-V curve, as shown in **Figure 3b**. When exposed to optical pulsing at moderate intensity (~7×10^8 W/cm^2), the tunneling behavior changes dramatically. The I-V curve becomes increasingly linear (**Figure 3c**) and the developed high F-N nonlinearity disappears (**Figure 3d**). This suggests a transition to one- or two-photon photoemission.[29, 30] In the photon-driven regime, the I-V curve should become increasingly linear as the barrier is undisturbed.[36] However, at optical power densities >1.4×10^9 W/cm^2, we observe a clear deviation from this photon-driven regime, with the measured I-V profiles adopting an unexpected (**Figure 3e**) and more F-N-like tunneling regime (V>1V) (**Figure 3f**). F-N tunneling is induced by a strong electric field and should not be solely induced by the bias voltage according to our findings in Figure 3a. We attribute this anomalous behavior to a new field-driven tunneling mode created by the superposition of static- and optical-fields.

To confirm the optical-field-driven mechanism observed, the power-dependent photocurrent, at a fixed bias voltage (+2V), was measured. Here we observed two distinct photoemission behaviors at the resonant and non-resonant wavelength. At a non-resonant wavelength of 730 nm, the photoemission current—light field strengthen (I-P) curve shows a known power-law dependence (I~P^2), as reported elsewhere, indicating multiphoton

photoemission[29, 30] (Figure S2). However, at the resonant wavelength of 880 nm, the I-P curve adopts a dramatically different form from the expected power-law scaling. As shown in **Figure 4a**, the I-P adopts three distinct regimes. At low power (<0.6 mW), the profile is nearly a third-order power-law scaling (purple line in Figure 4a, $I \sim P^3$). As one electron is required to absorb just two photons (photon energy, 1.41 eV) to overcome the Schottky barrier, we attribute the third power-law scaling to a possible hybrid mechanism involving both multiphoton photoemission and photo-assisted tunneling from resonantly excited states. At medium power (<1 mW), the curve deviated from this 3-photon scaling to a lower power order scaling (~1), with a slight decrease (~ 10%) in the measured photocurrent. The space-charge effect may account for this reduction.[37, 38] However, as the photocurrent is < 12 pA, which corresponds to less than one electron per pulse, and as the photocurrent increases again at elevated powers (1.2mW), it is likely that the space-charge effect can be eliminated given the low charges density involved. We noted that, following the decrease in photocurrent, at higher power (>1.2 mW), the profile behaves much more nonlinearly and tends to an $I \sim P^7$ order (red line, Figure 4a) that is here observed for the first time. This high nonlinearity is corroborated in **Figure 4b** by polarization dependence photocurrent measurements (orange points) where the date can be fitted to a $\cos^{14}(\theta)$ (red line). Here, the Keldysh parameter was used to further estimate the magnitude of the optical-field required to support the quasistatic electron tunneling, and is given by[39]

$$\gamma = \omega\sqrt{2m\phi}/e\beta F_0$$

where ω is optical frequency, ϕ is the height of Schottky barrier, m is the mass of the electron and e is its charge, F_0 is the incident optical-field strengthen, and β is the

optical-field enhancement factor of the nanogap of the MIM structure. Recently, it has been observed that the transition to tunneling behavior occurs when $\gamma = \sim 2$.[17, 20] In this work, for a 1.4×10^9 W/cm^2, 880 nm incident laser, the calculated $\gamma \sim 1.6$, further supporting the optical-field-driven electron tunneling regime observed.

The deviation of the I-P curve from power-law scaling has been widely investigated both experimentally and theoretically.[17, 20, 40, 41] Near the transition from power-law scaling, the strength of the optical-field is such that it readily disturbs the Schottky barrier. This induces the multiphoton channel to close, thereby reducing the nonlinearity.[33] This is consistent with the experimental results in the present work. Moreover, the fluctuation phenomenon of the I-P curve has been theoretically associated with the interference of electron wavepackets that coherently emit from two adjacent optical-cycle of the laser pulse.[37, 38] It should be noted that this only occurs in the optical-field-driven regime. However, such an I-P fluctuation phenomenon has seldomly been experimentally observed, primarily as a result of electron wavepacket decoherence, driven by environmental factors linked to necessarily long-distance propagation. The present MIMs device structure benefits from nanoscale propagation distances of <10 nm, allowing for stable access to the coherent nature of the optical-field-driven tunneling electrons, and thus, the coherent phenomenon can be observed.

The present MIM nano-junctions can be optimized by reducing the Schottky barrier further by incorporating additional low work function materials, such as emerging two-dimensional electrodes, and increasing the nonlinearity through the use of semiconducting electrodes. There are also further opportunities in using other dielectric materials such as 2D h-BN in order to further enhance the local fields. With continued reduction in the gap dimensions, as

well as an increased wavelength, such systems will provide a unique platform upon which to explore the transition of nanogap electron propagation from the quiver to the sub-cycle regime. The present device also provides a promising means of constructing two barrier structures, and thus a way to realize some of the first optical-field-driven resonant tunneling structures.

Here we have explored the detailed transport behavior in ultrafast laser-driven tunneling currents through a vertically constricted MIM tunneling junction with dimensions of just a few nanometers. The measured I-P properties firmly indicate a high nonlinearity up to 14 which suggests novel inter-cycle electron packet interference. These results demonstrate that MIM structures afford a unique platform upon which to establish, measure and manipulate coherent electron tunneling driven by optical-fields. These findings represent encouraging progress towards a new class of electronic nanodevices that operate via finely tunable electron dynamics. Such MIMs systems and the transport they support contribute promising research and practical directions in the ongoing efforts to shrink electronics ever further. These findings highlight that optical-field-driven inelastic tunneling may be a promising approach for realizing attosecond light sources with these experimental observations motivating future theoretical efforts to describe mesoscopic electron systems at the intersection between attosecond optics and quantum plasmonics.

Acknowledgements

The authors acknowledge funding from the National Key R&D Program of China (Grant No. 2016YFA0202001), the National Natural Science Foundation of China (Grant No. 11427808,

51972072 and 51602071), the Key Research Program of the Chinese Academy of Sciences (grant no. ZDBS-SSW-JSC002), CAS Interdisciplinary Innovation Team (grant no. JCTD-2018-03), and the Strategic Priority Research Program of the Chinese Academy of Sciences (grant no. XDB50020200 and XDPB06).

Conflict of Interest

The authors declare no conflict of interest.

References

[1] E. Goulielmakis, V. S. Yakovlev, A. L. Cavalieri, M. Uiberacker, V. Pervak, A. Apolonski, R. Kienberger, U. Kleineberg, F. Krausz, *Science* **2007**, 317, 769.

[2] S. Kumaragurubaran, T. Takahashi, Y. Masuda, S. Furuta, T. Sumiya, M. Ono, T. Shimizu, H. Suga, M. Horikawa, Y. Naitoh, *Applied Physics Letters* **2011**, 99, 263503.

[3] W. H. Kim, C. S. Park, J. Y. Son, *Carbon* **2014**, 79, 388.

[4] J. Yao, L. Zhong, Z. Zhang, T. He, Z. Jin, P. J. Wheeler, D. Natelson, J. M. Tour, *Small* **2009**, 5, 2910.

[5] C. He, Z. Shi, L. Zhang, W. Yang, R. Yang, D. Shi, G. Zhang, *ACS Nano* **2012**, 6, 4214.

[6] H. R. Park, X. S. Chen, N. C. Nguyen, J. Peraire, S. H. Oh, *Acs Photonics* **2015**, 2, 417.

[7] L. N. Tripathi, Y. M. Bahk, G. Choi, S. Han, N. Park, D. S. Kim, *Applied Physics Express* **2016**, 9, 032001.

[8] J. Keller, G. Scalari, S. Cibella, C. Maissen, F. Appugliese, E. Giovine, R. Leoni, M. Beck, J. Faist, *Nano Lett* **2017**, 17, 7410.

[9] M. Kim, E. Pallecchi, R. J. Ge, X. H. Wu, G. Ducournau, J. C. Lee, H. Happy, D. Akinwande, *Nature Electronics* **2020**, 3, 479.

[10] J. W. Han, D. I. Moon, M. Meyyappan, *Nano Lett* **2017**, 17, 2146.

[11] F. Krausz, M. Ivanov, *Reviews of Modern Physics* **2009**, 81, 163.

[12] D. J. Park, B. Piglosiewicz, S. Schmidt, H. Kollmann, M. Mascheck, C. Lienau, *Phys Rev Lett* **2012**, 109, 244803.

[13] G. Herink, D. R. Solli, M. Gulde, C. Ropers, *Nature* **2012**, 483, 190.

[14] M. Kruger, M. Schenk, P. Hommelhoff, *Nature* **2011**, 475, 78.

[15] D. R. Ward, F. Huser, F. Pauly, J. C. Cuevas, D. Natelson, *Nat Nanotechnol* **2010**, 5, 732.

[16] B. Piglosiewicz, S. Schmidt, D. J. Park, J. Vogelsang, P. Groß, C. Manzoni, P. Farinello, G. Cerullo, C. Lienau, *Nature Photonics* **2013**, 8, 37.

[17] P. Zimmermann, A. Hotger, N. Fernandez, A. Nolinder, K. Muller, J. J. Finley, A. W. Holleitner, *Nano Lett* **2019**, 19, 1172.

[18] T. Rybka, M. Ludwig, M. F. Schmalz, V. Knittel, D. Brida, A. Leitenstorfer, *Nature Photonics* **2016**, 10, 667.

[19] M. Ludwig, G. Aguirregabiria, F. Ritzkowsky, T. Rybka, D. C. Marinica, J. Aizpurua, A. G. Borisov, A. Leitenstorfer, D. Brida, *Nature Physics* **2019**, 16, 341.

[20] M. Garg, K. Kern, *Science* **2020**, 367, 411.

[21] C. Karnetzky, P. Zimmermann, C. Trummer, C. Duque Sierra, M. Worle, R. Kienberger, A. Holleitner, *Nat Commun* **2018**, 9, 2471.

[22] Y. Yang, M. Turchetti, P. Vasireddy, W. P. Putnam, O. Karnbach, A. Nardi, F. X. Kartner, K. K. Berggren, P. D. Keathley, *Nat Commun* **2020**, 11, 3407.

[23] H. Chalabi, D. Schoen, M. L. Brongersma, *Nano Lett* **2014**, 14, 1374.

[24] F. P. Garcia de Arquer, A. Mihi, D. Kufer, G. Konstantatos, *ACS Nano* **2013**, 7, 3581.

[25] M. L. Huang, Y. C. Chang, C. H. Chang, T. D. Lin, J. Kwo, T. B. Wu, M. Hong, *Applied Physics Letters* **2006**, 89.

[26] R. H. Fowler, L. Nordheim, *Proceedings of the Royal Society of London Series a-Containing Papers of a Mathematical and Physical Character* **1928**, 119, 173.

[27] E. L. Murphy, R. H. Good, *Physical Review* **1956**, 102, 1464.
[28] M. Vahdani Moghaddam, P. Yaghoobi, G. A. Sawatzky, A. Nojeh, *ACS Nano* **2015**, 9, 4064.
[29] L. Seiffert, T. Paschen, P. Hommelhoff, T. Fennel, *Journal of Physics B-Atomic Molecular and Optical Physics* **2018**, 51, 134001.
[30] P. Musumeci, L. Cultrera, M. Ferrario, D. Filippetto, G. Gatti, M. S. Gutierrez, J. T. Moody, N. Moore, J. B. Rosenzweig, C. M. Scoby, G. Travish, C. Vicario, *Phys Rev Lett* **2010**, 104, 084801.
[31] W. P. Putnam, R. G. Hobbs, P. D. Keathley, K. K. Berggren, F. X. Kärtner, *Nature Physics* **2016**, 13, 335.
[32] H. Yanagisawa, C. Hafner, P. Dona, M. Klockner, D. Leuenberger, T. Greber, M. Hengsberger, J. Osterwalder, *Phys Rev Lett* **2009**, 103, 257603.
[33] P. Hommelhoff, C. Kealhofer, M. A. Kasevich, *Phys Rev Lett* **2006**, 97, 247402.
[34] S. Nirantar, T. Ahmed, G. Ren, P. Gutruf, C. Xu, M. Bhaskaran, S. Walia, S. Sriram, *Nano Lett* **2018**, 18, 7478.
[35] J. J. Odwyer, *Journal of Applied Physics* **1966**, 37, 599.
[36] M. Turchetti, M. R. Bionta, Y. J. Yang, F. Ritzkowsky, D. R. Candido, M. E. Flatte, K. K. Berggren, P. D. Keathley, *Journal of the Optical Society of America B-Optical Physics* **2021**, 38, 1009.
[37] D. Diesing, M. Merschdorf, A. Thon, W. Pfeiffer, *Applied Physics B* **2004**, 78, 443.
[38] A. Thon, M. Merschdorf, W. Pfeiffer, T. Klamroth, P. Saalfrank, D. Diesing, *Applied Physics A: Materials Science & Processing* **2004**, 78, 189.
[39] L. V. Keldysh, *Soviet Physics Jetp-Ussr* **1965**, 20, 1307.
[40] H. R. Reiss, *Physical Review A* **1980**, 22, 1786.
[41] R. Bormann, M. Gulde, A. Weismann, S. V. Yalunin, C. Ropers, *Phys Rev Lett* **2010**, 105, 147601.

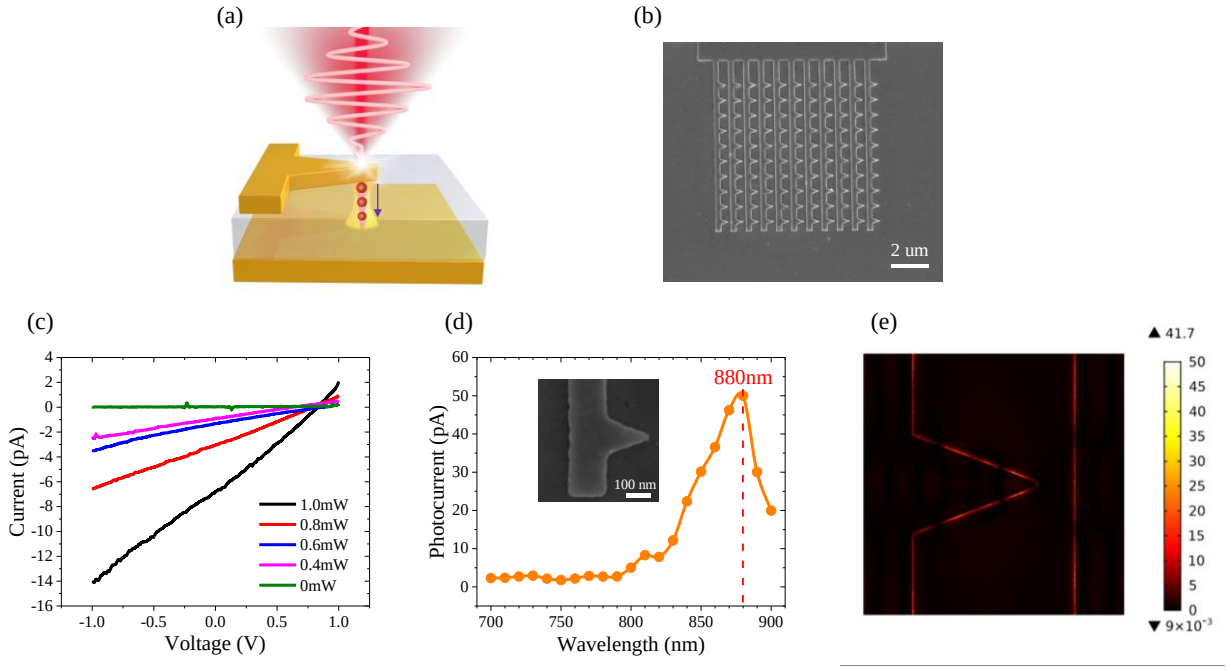

Figure 1. Typical fabricated antenna coupled metal-insulator-metal (MIM) nano-junction. (a) Schematic depiction of the MIM device with electron emission being stimulated by a femtosecond laser pulse. (b) A scanning electron microscope (SEM) image of a representative fabricated MIM device. (Scale bar: 2 μm). (c) Typical measured I-V characteristics of a MIM device without laser illumination (0 mW) and as a function of different laser power. (d) Photocurrent spectra of the MIM device with different laser wavelengths. The measured photocurrent spectrum has a peak near 880 nm. Inset: SEM image of the measured device. (Scale bar: 100 nm). The width of the stripe is ~300±30 nm, the base of the nanotriangle is ~300±20 nm, and the height is ~400±30 nm. (e) Simulated electromagnetic field distribution in Ti/Au-Al_2O_3 interface of the MIM device. The maximum of field enhancement is 41.7 at λ=880 nm.

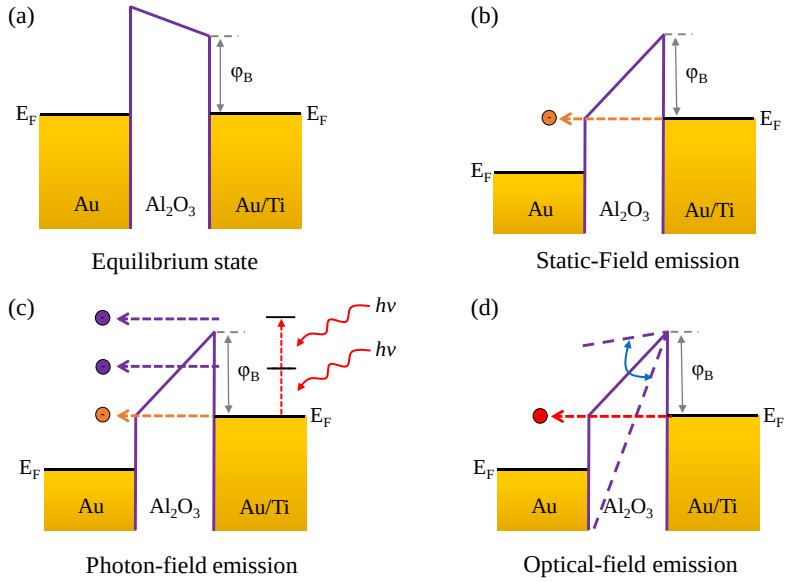

Figure 2. MIM nano-junction operation principle. (a) Energy band diagram for the equilibrium state (no bias, no illumination). Where φ_B is the barrier height (~1.73 eV), E_f is the Fermi level. (b) Energy band diagram during static-field emission. Depending on the bias voltage, the static-field-driven tunneling may transit from direct tunneling (rectangular barrier) to F-N tunneling (triangular barrier). (c) Energy band diagram for photon-field emission, including multiphoton photoemission and photo-assisted tunneling. *hv* is the photon energy. (d) Energy band diagram for optical-field emission.

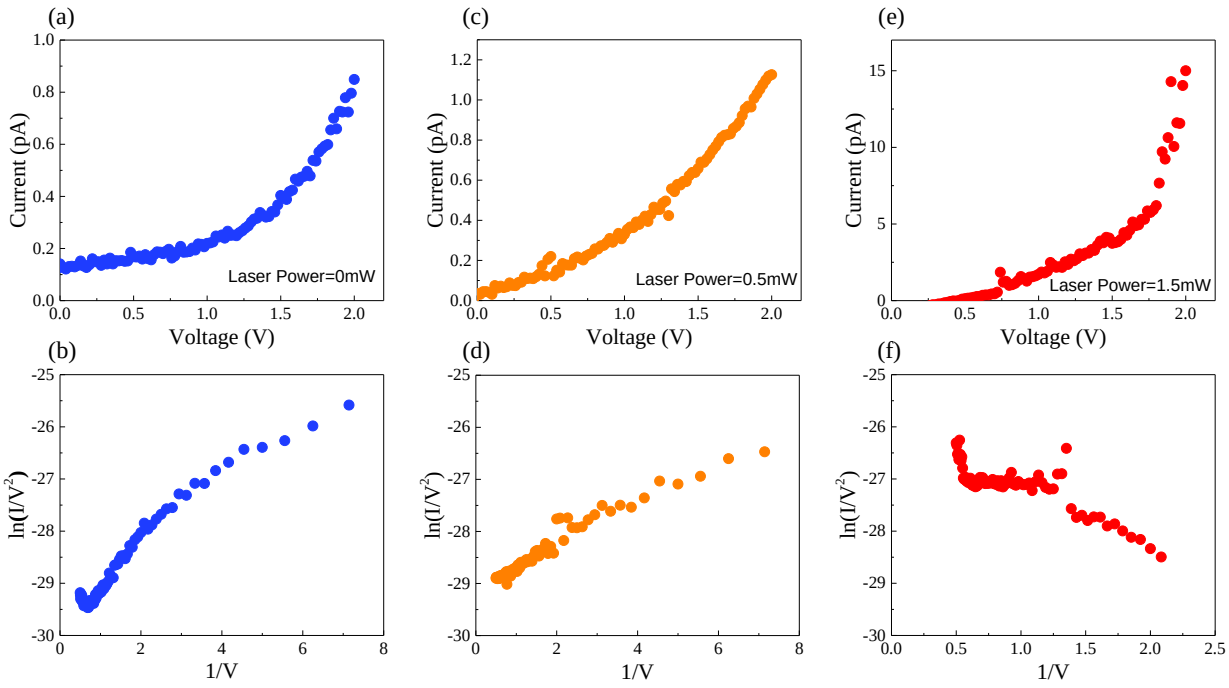

Figure 3. Transport characteristic as a function of laser power. Measured I-V curve (a) without laser illumination (0 mW), and with optical power of (c) 0.5 mW, and (e) 1.5mW. (b) (d) (f) are the corresponding F-N plots, respectively.

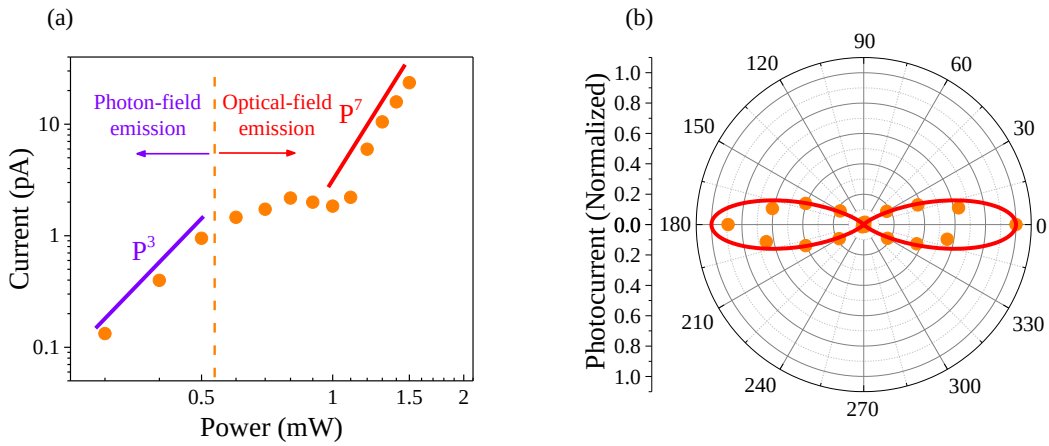

Figure 4. MIM nano-junction photon response. (a) Laser-induced tunneling current as a function of increasing laser power at the resonant wavelength (880 nm). (b) Photocurrent polarization-dependent at λ=880 nm (orange points), exhibiting a $\cos^{14}(\theta)$ angular dependence (red line). Angle 0° of polarization is parallel to the height of the nanotriangle.

Supporting Information

S1: MIM nano-junction fabrication

Electron beam lithography (EBL) was used to fabricate the MIM nano-junctions on 525 (±25) μm thick silicon (phosphorus doping, 1-10 ohm-cm) substrate coated with a 285 (±20) nm SiO_2 layer (thermal oxide). This was achieved using a positive electron beam resist (polymethylmethacrylate (PMMA) with a molecular weight of 950 K) that was spin-coated at 4000 rpm for 60 s which was soft-baked for 120 s at 180 °C. The bottom electrode was similarly patterned by EBL at 100 kV and an exposure dose of 900 μC/cm^2. Resist were developed by rinsing the exposed samples in a mixture of 3:1 isopropanol alcohol (IPA) and methyl isobutyl ketone (MIBK) for 60 s, and then fixing in IPA for 30 s. A 60 nm thick Au layer was deposited by electron-beam evaporation (OHMIKER-50B). The PMMA resist layer was lift-off removed in acetone (≥99.5%, Sinopharm Chemical Reagent Co., Ltd.) for 20 min in a heated water bath at 80 °C. This electrode was then overgrown with an 8 nm-thick Al_2O_3 layer by atomic layer deposition (ALD, SENTECH Instruments GmbH). Finally, the above EBL process was repeated to fabricate the array of nanotriangle antennas above the bottom electrode. The top electrodes consisted of a series of 11 parallel Au stripes (3 nm Ti/60 nm Au) with asymmetric nanotriangle structures, which are oriented in an orthogonal direction of the bottom electrodes. The base of the nanotriangle is h ~ (300 ± 20) nm, with height is l ~ (400 ± 30) nm.

S2: Characterization and electronic measurements

The morphologies of the MIM nano-junctions were characterized by SEM (FEI NOVA nano-430). The I-V characteristics of the MIM nano-junctions were measured with Keithley 2636B source measure unit. Incident light from a femtosecond laser source (Chameleon Ultra Laser System, Coherent) was focus on the sample using 50× Olympus objective (0.55 NA, 8.2 WD) resulting with an FWHM spot size of ~2.5 μm. Optical images were obtained under the same objective and recorded using a CCD camera (MER-310-12UC, Daheng Optics) to confirm the laser position on the antennas. All measurements were performed at atmospheric pressure at room temperature.

S3: Simulations

Finite element simulations were conducted in the COMSOL software to investigate the electromagnetic field distributions and field enhancement with the MIM nano-junctions.

S4:

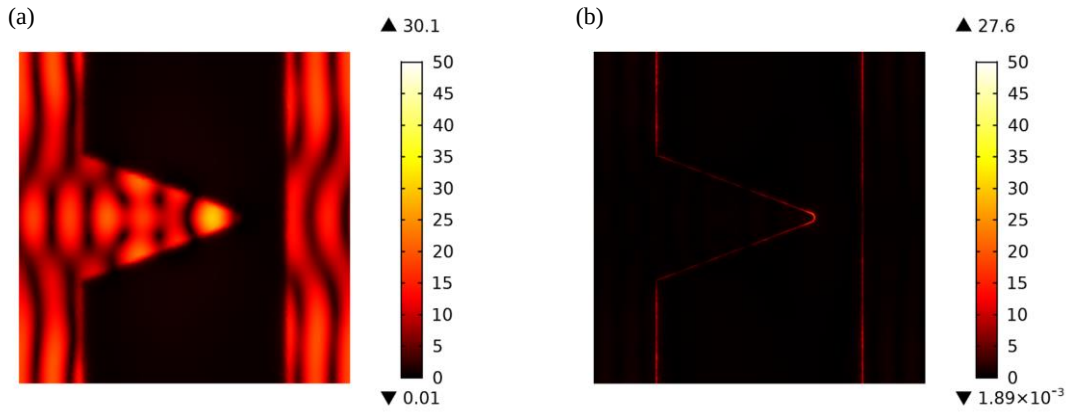

Figure S1. (a) Electromagnetic field distribution at the Al_2O_3-Au interface. The maximum of field enhancement (β=30.1) is lower than the Ti/Au-Al_2O_3 interface at λ=880 nm. (b) Electromagnetic field distribution at the Ti/Au-Al_2O_3 interface of the MIM device, with a maximum field enhancement of 27.6 at λ=730 nm.

S5:

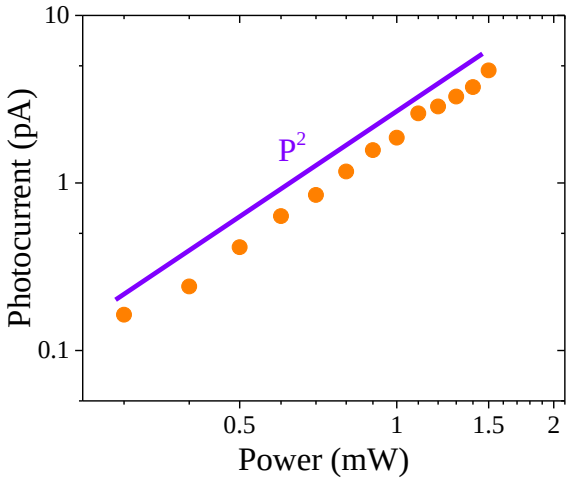

Figure S2. Laser-induced tunneling current as a function of increasing laser power at the non-resonant wavelength (730 nm). The curve is a two-order power-law scaling (purple line, $I \sim P^2$), corresponding multiphoton photoemission.

S6:

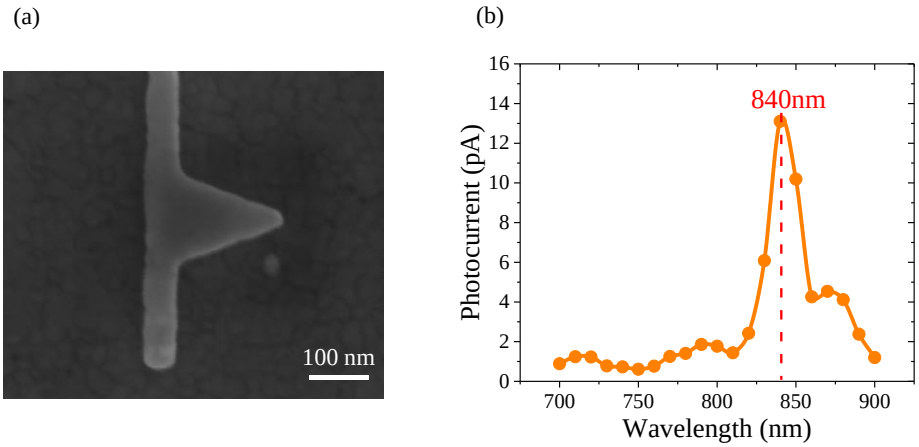

Figure S3. (a) SEM image of a single fabricated MIM device formed with 100 nm width stripes. (b) Photocurrent spectra of this MIM device as a function of different laser wavelengths, demonstrating a resonant peak near 840 nm.

S7:

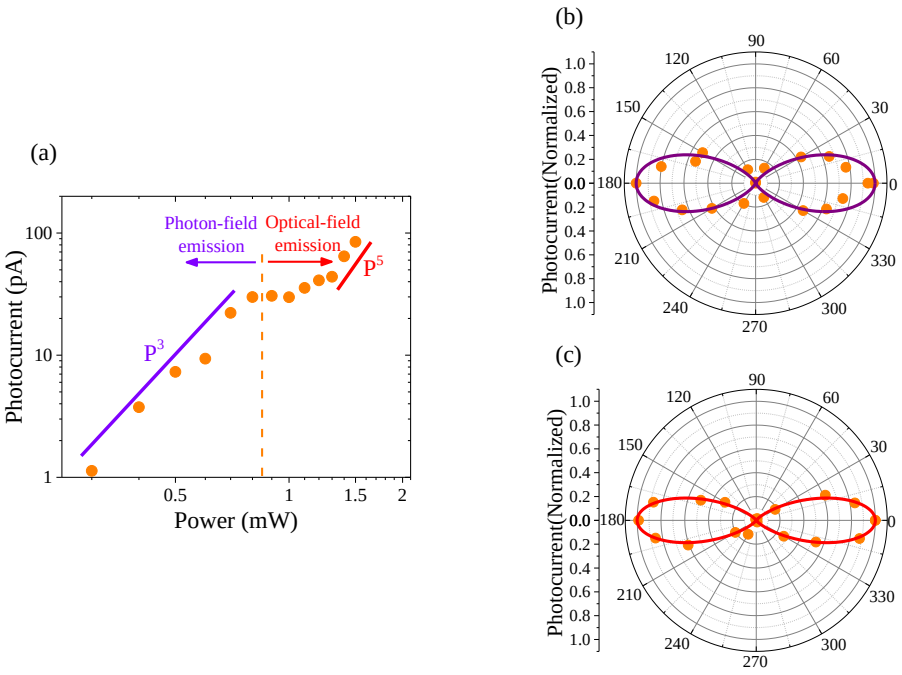

Figure S4. (a) Laser-induced tunneling current as a function of increasing laser power at 840 nm. The I-P curve behaves similar characteristics with three different regimes. (b) Photocurrent polarization-dependent at λ=840 nm at 0.5 mW (orange points), exhibiting a $\cos^6(\theta)$ angular dependence (purple line). Angle 0° of polarization is parallel to the height of the nanotriangle. (c) Photocurrent polarization-dependent at λ=840 nm at 1.4 mW (orange points), exhibiting a $\cos^{10}(\theta)$ angular dependence (red line).